ACS APPLIED MATERIALS & INTERFACES

Research Article

www.acsami.org

Ultrasonic-Assisted Synthesis of Surface-Clean TiB_2 Nanoparticles and Their Improved Dispersion and Capture in Al-Matrix Nanocomposites

Marc Estruga,[†] Lianyi Chen,[‡] Hongseok Choi,[‡] Xiaochun Li,[‡] and Song Jin*[,†]

[†]Department of Chemistry, University of Wisconsin-Madison, 1101 University Avenue, Madison, Wisconsin 53706, United States

[‡]Department of Mechanical Engineering, University of Wisconsin-Madison, 1513 University Avenue, Madison, Wisconsin 53706, United States

Supporting Information

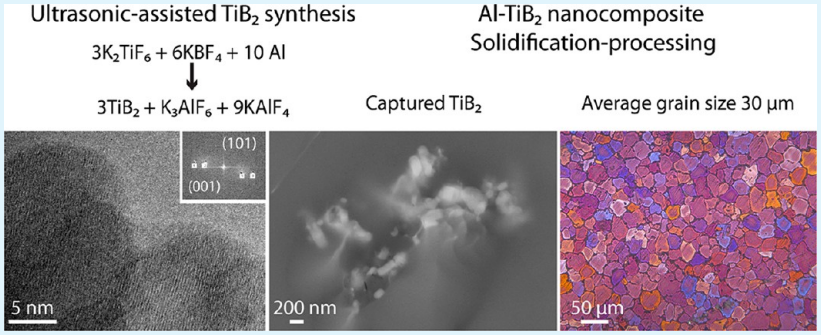

ABSTRACT: Metal-matrix nanocomposites (MMNCs) have great potential for a wide range of applications. To provide high performance, effective nanoparticle (NP) dispersion in the liquid and NP capture within the metal grains during solidification is essential. In this work, we present the novel synthesis and structural characterization of surface-clean titanium diboride (TiB_2) NPs with an average particle size of 20 nm, by ultrasonic-assisted reduction of fluorotitanate and fluoroboride salts in molten aluminum. The high-intensity ultrasonic field restricts NP growth. Using a master nanocomposite approach, the as-prepared TiB_2 NPs are effectively incorporated into A206 alloys during solidification processing because of their clean surface, showing partial capture and significant grain refinement.

KEYWORDS: *TiB_2 nanoparticles, metal-matrix nanocomposites, dispersion, wettability, ultrasonic processing*

1. INTRODUCTION

High-strength lightweight Al and Mg alloys are promising materials for structural, transportation, aerospace and military applications. The significant weight reduction with respect to current choices would help to meet low energy consumption requirements and reduce CO_2 emissions of transportation industry. However, their mechanical properties still fall short of the requirements to be widely used in large-scale manufacturing processes. In this context, nanoparticle (NP)-reinforced metal-matrix nanocomposites (MMNCs) are hybrid materials consisting of a continuous metallic matrix with embedded inorganic nanomaterials. This results in the desired combination of mechanical properties: enhanced strength, due to the load transfer of hard inorganic nanomaterials and Orowan strengthening, coupled with a reasonably high ductility, delivered by the metal.[1−3] Current fabrication methods for MMNCs are mostly based on powder metallurgy, which have shown promising results at laboratory scale, but are not suitable to be scaled up to industrial economically viable processes.[1]

Since solidification-processing methods (e.g., casting) are the most cost-effective approach for large-scale processing of metals, there is a strong interest for the development of casting approaches to fabricate MMNCs.[4] Some researchers have explored in situ reinforcement fabrication methods,[1,5] but it is difficult to control particle size at the nanoscale, and the processes are not easily scalable. Thus, ex-situ methods (that is, adding the reinforcement NP to the liquid metal) still provide more advantages than drawbacks in this regard. One of the challenges in this nanomanufacturing technology is the effective incorporation of the reinforcement material into the liquid alloy, which requires good wetting between the solid NPs and the metal fluid.[6] Because of the much higher surface area of nanomaterials, the surface chemistry and interfacial tension play a key role in particle-metal interactions. For example, NPs of conventional metal oxides such as Al_2O_3 show poor wetting with molten Al.[7] In this context, nanomaterial wetting behavior with aqueous fluids, organic solvents, and polymers at low temperature can be controlled by tailoring the NPs' surface

Received: July 8, 2013
Accepted: August 19, 2013
Published: August 19, 2013

functionalization,[8,9] while nanomaterial wetting by molten metal still remains poorly understood. Another limitation for a successful large-scale processing of MMNCs is caused by the difficulty to obtain effective NP capture during the solidification processing, that is, to ensure the homogeneous distribution of the reinforcement NPs inside the primary metal grains, which will greatly improve the mechanical properties of the resulting nanocomposite. To overcome those restrictions, first, the interfacial energy between the NP and the molten metal must be small, so that there is a good wetting between the two materials and the reinforcement can be easily dispersed in the liquid metal.[10] Moreover, as the molten metal solidification front approaches the NP, the van der Waals repulsive potential between the solidification front and the NP has to be smaller than the thermal energy of the NPs to promote its capture.[11,12] The two attributes of the NPs that affect the van der Waals interaction are (i) the Hamaker constant (A, an indicator of the magnitude of the interaction between two solids separated by a fluid); and (ii) the NP diameter. Thus, by choosing materials with high Hamaker constants and small nanoscale diameters, NP capture can be promoted. Moreover, the extreme environment during molten metal processing places severe constraints on the nanomaterials that can be used. For example, the high temperature of the casting process (~ 700 °C) and the high reduction potential of metallic Al rule out many oxides that will chemically react with Al (such as TiO_2, ZrO_2, CuO, ZnO, etc.).

Nanoscaled metal borides exhibit a wide range of properties, including conduction, luminescence, thermoelectricity, magnetism, and ultrahardness, among others, that makes them interesting in the fields of refractory conductive ceramics, superconductors, and hard materials.[13] In this context, titanium diboride (TiB_2) NPs are an excellent candidate as the reinforcing element in MMNCs because TiB_2 (i) is thermodynamically stable in liquid Al;[14] (ii) has a low interfacial energy (and thus, good wettability) with Al,[15,16] which ensures effective NP incorporation in the melt; and (iii) has a Hamaker constant close to that of the liquid Al, which would promote NP capture by Brownian motion during metal front solidification.[12] However, the commercially available nanosized TiB_2 has a surface carbon-coating inherent to the arc-plasma synthetic process, which promotes the oxidation reactions and hinders NP incorporation into the metal melt, making it not useful for reinforcing material in solidification-processing of MMNCs. Laboratory-scale synthetic methods for nanostructured TiB_2 often involve air-sensitive precursors and tedious multistep procedures,[17] or highly pressurized reactors.[18] Alternatively, mechanochemical methods (e.g., ball milling) are promising alternatives, but issues with large particle size distribution and surface impurities must be addressed.[13,19] In this context, the reduction of Ti and B salts in molten Al has been proposed as viable TiB_2 synthetic process; however, it normally yields microsized particles that are not useful for superior strengthening of composites.[20−24] In this study, we have developed a novel synthetic approach by coupling the reduction of potassium hexafluorotitanate (K_2TiF_6) and potassium tetrafluoroboride (KBF_4) in molten Al with a high intensity ultrasonic field that restricts the particle growth, resulting in small TiB_2 NPs. Because of this synthetic advance, NPs have been effectively incorporated and dispersed into A206 alloys, with a significant fraction captured inside the primary Al grains.

2. EXPERIMENTAL SECTION

2.1. Reagents. Potassium hexafluorotitanate (K_2TiF_6, > 98%, CAS number 16919-27-0), potassium tetrafluoroboride (KBF_4, > 96%, CAS number 14075-53-7), calcium fluoride (CaF_2, > 99.5%, CAS number 7789-75-5), aluminum micropowder (Al, ≤ 30 μm in diameter, ≥ 99%, CAS number 7429-90-5), and hydrochloric acid (HCl, 37% in H_2O, CAS number 7647-01-0) were purchased from Sigma Aldrich and used as received. Commercial TiB_2 nanopowder (+95%, 58 nm in diameter, U.S. Research Nanomaterials, Inc.) was used as received. Pure metals and standard alloys (A1350, Al6Ti, Cu, Mg, B206, and A206 were supplied by Eck Industries, Inc. (Manitowoc, WI, U.S.A.).

2.2. NP Synthesis. For a typical TiB_2 NP synthesis, K_2TiF_6 (10.68 g, 44.5 mmol), KBF_4 (11.16 g, 88.6 mmol), and CaF_2 (1.00 g, 12.8 mmol) were mixed and thoroughly hand-grinded in an agate mortar for 10 min. The powder mixture was then heated to 120 °C for 1 h to minimize its moisture level. In parallel, A1350 aluminum alloy (100 g) was heated up to 700 °C inside a graphite crucible placed in a resistance heating furnace, which was under continuous protective Ar flow.[25] Once the liquid metal reached constant temperature, the ultrasonic system, composed of a niobium C103 alloy waveguide (1.27 cm in diameter, 9.2 cm in length) coupled with a 20 kHz 600 W ultrasonic transducer (Misonix Inc., Newtown, CT, U.S.A.) was turned on. Peak to peak amplitude was adjusted to 50 μm, and the probe was submerged 0.5 cm deep into the melt. Then, the dry reagent mixture was added into the melt and reaction occurred immediately. The mixture was sonicated for 10 min (unless otherwise noted) at 700 °C, and the slug on the melt surface was removed before pouring the metal into a Cu plate mold for solidification. To isolate pure TiB_2 NPs, the Al matrix was dissolved in 20 vol. % aqueous HCl using an ice bath in a secondary container (***Caution!*** *The Al dissolution process is highly exothermic and causes sudden temperature increase*). The resulting TiB_2 NP suspension was centrifuged and thoroughly washed with water several times until the supernatant displayed neutral pH. Finally, TiB_2 NPs were dried overnight on a hot plate at 60 °C for further characterization and use.

2.3. Master Pellet Preparation. The as-prepared TiB_2 NPs were used to fabricate Al-TiB_2 master nanocomposite pellets (50 wt % in TiB_2) that would be further used to prepare the final nanocomposite with desired composition. Approximately 0.50 g of TiB_2 NPs were mixed with an equal mass of Al micropowder and thoroughly grinded for 10 min in an agate mortar. This powder mixture was manually compacted into a cylindrical alumina crucible (2.5 cm tall, 2 cm in diameter). Then, the crucible was introduced into a fused silica tube (2.5 cm in diameter, ~80 cm in length) placed in a tube furnace (Lindberg/Blue M) equipped with pressure and gas flow controls. The compacted samples were placed under dynamic vacuum at ~5 mTorr for 1 h at 150 °C to remove the moisture on the powder surface. Then, the system was heated up to 900 °C and kept at this temperature for 1 h under an Ar/H_2 coflow (200 sccm, 50 vol. %) at 760 Torr. After thermal treatment, the furnace was naturally cooled down to room temperature. The resulting cylindrical compact Al-TiB_2 pellets were easily removed from the crucible and used as NP feedstock in the casting experiments. For the control experiments, Al pellets were prepared using the Al micropowder without the TiB_2 NPs.

2.4. Ultrasonic-Assisted Al Casting Procedure. A206-TiB_2 nanocomposites were then prepared by melting the as-prepared TiB_2 master nanocomposite pellets into liquid A206, using the same ultrasonic-cavitation experimental setup used for NP synthesis. A206 alloy (156 g) was heated to 700 °C in a graphite crucible (7.77 cm tall, 3.6 cm inner diameter). Once the molten alloy reached constant temperature, the ultrasonic system was turned on. Peak to peak amplitude was adjusted to 50 μm, and the probe was submerged 0.5 cm deep into the melt. Three Al-TiB_2 master nanocomposite pellets (50 wt % TiB_2, about 3.2 g total weight) were introduced into the melt and the ultrasonic process was maintained for 30 min at 700 °C to disperse the NPs into the metal. Pure Al pellets were used to prepare the control A206 alloys. After the ultrasonic processing, the probe was lifted out of the melt, and the temperature of the melt was increased to 740 °C for casting into a steel permanent mold (preheated to 400 °C).

Samples were cut, grinded, and polished using SiC paper and alumina micropowder, respectively. Before microscopy imaging, the polished samples were ion-milled (Fischione F1010) to remove the remaining polishing colloids.

2.5. Characterization. Powder X-ray diffraction (XRD) patterns were collected on a Bruker D8 Advance Powder diffractometer using Cu $K_{\alpha 1}$ radiation. Scanning electron micrographs (SEM) were acquired using a LEO Supra 55 VP field emission microscope operating at 3 kV and Energy-dispersive X-ray spectroscopy (EDS) mapping was performed in a LEO 1530 SEM. NP suspension in ethanol was drop-casted onto Transmission Electron Microscopy (TEM) grids (Ted Pella, lacey carbon type-A on 300 mesh Cu grids, #01890-F). TEM was carried out using a Philips CM200UT electron microscope operating at 200 kV. Elemental analysis of the as-prepared alloys and nanocomposites was performed using Spark-Optical Emission Spectrometry (Thermo Scientific, ARL 3460). Grain size was calculated from polarized light micrographs of polished specimens after electroetching in a HBF_4 solution (1.8 wt % in H_2O at a constant potential of 22 V for 20 s).

3. RESULTS AND DISCUSSION

3.1. TiB_2 NP Synthesis. We have developed a novel synthetic approach to TiB_2 NPs by combining the reduction of potassium hexafluoride (K_2TiF_6) and potassium tetrafluoroboride (KBF_4) in molten Al with high intensity ultrasonic field. K_2TiF_6 and KBF_4 are interesting starting materials for the synthesis of TiB_2 because of the possibility to perform the reduction at lower temperature when compared to the titanium and boron oxides.[26] The main limitation of this reduction method is that, at best, it can only provide submicro-sized particles, which are less useful as reinforcement phase in metal matrix composites.[27,28] For these reasons, there is a strong interest in the synthesis of smaller TiB_2 NPs and their application as ceramic reinforcement for MMNCs.

In our approach, the combination of ultrasonic processing with aluminothermic reduction of titanium and boron fluorinated salts in molten Al results in the formation of phase-pure TiB_2. Right after the addition of the salt mixture to the molten metal under ultrasonic cavitation, the Al reacts with the K_2TiF_6 and KBF_4 exothermically:[26]

$$3K_2TiF_6 + 6KBF_4 + 10Al \rightarrow 3TiB_2 + K_3AlF_6 + 9KAlF_4 \quad (1)$$

The byproduct salt consists in a mixture of potassium fluoroaluminides like K_3AlF_6 or $KAlF_4$ plus other species such as AlF_3 and KF. This reaction happens immediately, as demonstrated by the fact that TiB_2 NPs can be obtained using reaction time as short as 5 min (data not shown). In addition, the phase, size, and morphology of the TiB_2 NPs have been found to be independent of the ultrasonic processing time in the 5−30 min range, so 10 min was selected as the standard.

At the process temperature (700 °C), the byproduct fluoroaluminide salt mixture is a liquid, forming a two-phase immiscible liquid system with molten Al. The addition of CaF_2 to the reagent mixture improves the separation of these two liquid phases by increasing their surface tension, thus eliminating the presence of K_3AlF_6, AlF_3, or $KAlF_4$ in the retrieved product powder after HCl washing. The phase purity of the NP product is confirmed by XRD (Figure 1a), which shows a perfect match with the standard hexagonal TiB_2 pattern (space group *P6/mmm*, JCPDS #65-8698) and no other phases were present within the XRD detection limit. Moreover, low magnification TEM (Figure 1b) shows the small particle size distribution, which ranges from 10 to 100 nm, while HRTEM (Figure 1c) confirms the TiB_2 phase at the nanoscale, since the lattice fringes measured on the fast Fourier transform (inset of Figure 1c) match the lattice parameters of the (101) and (001) TiB_2 planes (2.03 and 3.22 Å, respectively).

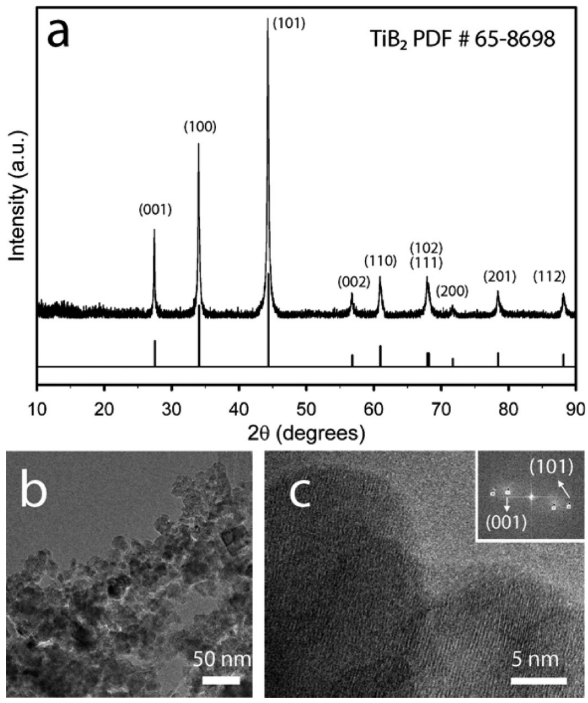

Figure 1. XRD (a), and TEM (b, c) characterization of the as-prepared TiB_2 NPs.

The ultrasonic processing is critical in producing NPs. Indeed, as shown in Figure 2, the ultrasonic-assisted TiB_2 synthesis leads to NPs of ~20 nm average diameter (Figure 2a and c), which are about 1 order of magnitude smaller than the particles prepared using mechanical stirring (Figure 2b and d). The contrast between these results suggests that the applied high-intensity ultrasonic field is responsible for the significant

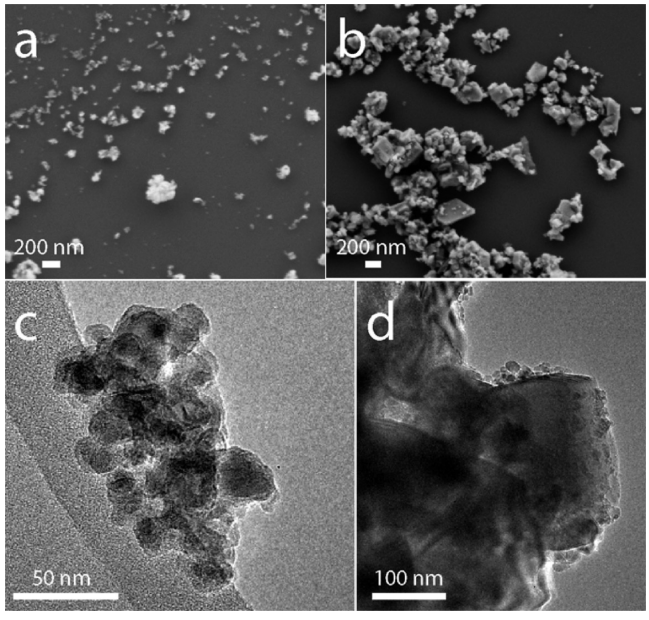

Figure 2. SEM and TEM of the TiB_2 powders obtained by sonication-assisted process (a, c) and conventional mechanical stirring (b, d).

dx.doi.org/10.1021/am402719p | ACS Appl. Mater. Interfaces 2013, 5, 8813−8819

particle size reduction. That mechanism can be explained by the extremely high temperature and pressure that is locally achieved because of acoustic cavitation.[29] These hot spots act as effective nucleation centers for TiB_2 particles resulting in much smaller particle size. Moreover, the acoustic streaming effects are known to promote the efficient mixing and diffusion of reactants. In our specific case, this leads to smaller and better-distributed molten salt reagent droplets within the Al melt, which result in larger contact area between the reactants, and thus, enhanced TiB_2 NP nucleation.

3.2. Al-TiB_2 Master Nanocomposite Preparation. If the as-prepared TiB_2 NPs are directly fed as nanopowder into molten A206 alloy to fabricate the nanocomposite by solidification processing, they react with the trace amount of O_2 near the surface of the melt. This results in the oxidation of TiB_2 into TiO_2, which is not a good reinforcement material because it is not stable in molten Al environment. The oxidation issue during the feeding of NPs into molten metal is also encountered in other nonoxide ceramics such as TiCN, SiC, and so forth.

To provide a more convenient method for NP feeding into the melt, we adopt the concept of master nanocomposite alloy.[30] In this approach, the self-prepared TiB_2 NPs are first mixed with Al micropowder (50 wt % loading), and the mixture is packed and annealed under Ar/H_2 protective atmosphere at 900 °C, resulting in a robust and compact Al-TiB_2 pellet (Figure 3 inset) that is much easier to manipulate than the

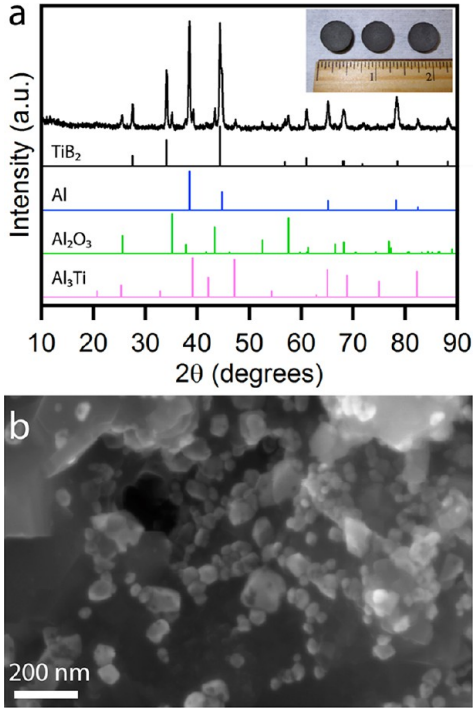

Figure 3. XRD pattern (a), photograph (inset of a, ruler scale in inches) and SEM micrograph (b) of the fractured cross-section of the Al-TiB_2 master nanocomposite pellets.

initial nanopowder material. XRD analysis (Figure 3a) confirms that the major phases are TiB_2 and Al (JCPDS # 65-8698 and 65-2869, respectively) with traces of Al_2O_3 and Al_3Ti (JCPDS # 46-1212 and 37-1449, respectively) that might come from the alumina oxidation layer that exists in commercial Al micro-particles and its reaction with the Al-TiB_2 matrix under such a high reducing environment at high temperature.

TiB_2 NP distribution in master nanocomposite pellets is reasonably good, considering the high loading of the ceramic reinforcement (50 wt %). As shown in Figure 3b, the NPs are homogeneously distributed in the Al matrix, and the high NP concentration implies that some particles are forming small clusters of about 200 nm in diameter, which contain between 10 and 20 individual NPs. Moreover, Ti has been detected by EDS (38 at. %), confirming the presence of TiB_2 in the master nanocomposite pellets. B element is too light to be quantified by EDS technique.

The good incorporation and distribution of NPs into the Al matrix shown in Figure 3b suggests that the as-prepared TiB_2 NPs have good wetting with Al, which promotes dispersion in the matrix.[31] This behavior is critical for effective NP dispersion into the alloys and is not seen in other more common reinforcement materials such as Al_2O_3 or TiCN. In contrast, commercial TiB_2 NPs (from U.S. Research Nanomaterials, Inc.) were also tested under the same conditions for master pellet preparation, which resulted in a loose powder (Figure 4,

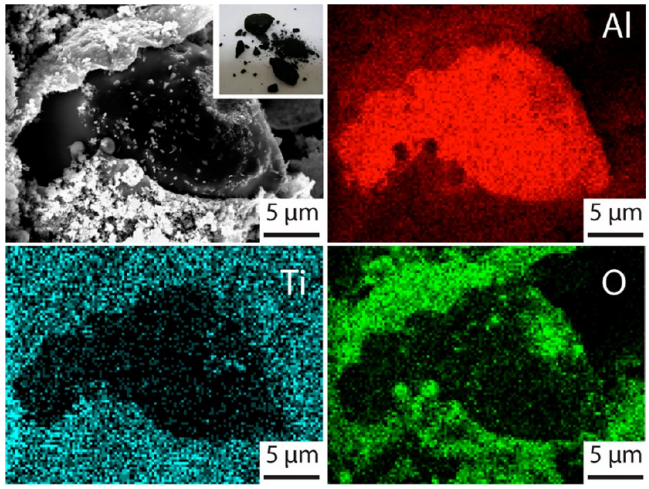

Figure 4. SEM micrograph and EDS mapping (Al, Ti, O) and digital photograph (inset) of the master nanocomposite using commercial TiB_2 NPs.

inset photograph) because of the poor wettability. This is caused by the presence of a carbon layer on the NP surface, which prevents an intimate contact between the TiB_2 and Al during the high temperature annealing process. Moreover, the poor wetting behavior resulted in NP oxidation by the trace O_2, as shown by EDS mapping (Figure 4). We attribute the superior dispersion behavior of the TiB_2 NPs synthesized herein to the clean, carbon-free surface shown in high-resolution TEM (Figure 1c).

3.3. A206-TiB_2 Nanocomposite Casting. Because of the successful wetting of the TiB_2 NPs with Al during master nanocomposite pellet preparation, the Al-TiB_2 compact can be effectively dispersed during ultrasonic-assisted casting. First, the A206 alloy was heated up to 700 °C, and the melt was subjected to ultrasonic irradiation. Immediately, the Al-TiB_2 pellets were added to the melt surface, and after 5 min they were completely dispersed into the liquid alloy. This process is facilitated by the pre-existing good Al-TiB_2 wetting achieved during the pellet preparation step. After 30 min total sonication time, the TiB_2 NPs are homogeneously dispersed, allowing the

melt to be poured into a preheated stainless steel permanent mold. Four different sets of samples were prepared following this procedure, and their compositions are summarized in Table 1.

Table 1. Elemental Analysis of the As-Prepared A206 Alloys and Nanocomposites[a]

sample	Al	Cu	Mg	Ti
(i) Control A206	94.75	4.30	0.24	0.17
(ii) A206 + 1TiB_2	94.25	3.87	0.25	0.98
(iii) Control A206 + 0.2Mg + 0.1Ti	94.70	4.12	0.45	0.20
(iv) A206 + 0.2Mg + 0.1Ti + 1TiB_2	93.80	4.13	0.44	1.03

[a]Values are shown in wt %.

Effective NP incorporation is confirmed for both nanocomposites (ii and iv), as demonstrated by the fact that the overall Ti content matches the Ti already present in the A206 matrix plus the additional 1 wt % TiB_2 added as reinforcement material. Optical and SEM micrographs of the Control A206 sample show the typical θ-Al_2Cu continuous network distributed within the Al matrix, a well-known microstructure for Al−Cu alloy system (data not shown).[32]

Microstructure analysis of the A206 + 1 wt % TiB_2 nanocomposite (Figure 5) shows that a fraction of the TiB_2 NPs are pushed to the grain boundaries, together with the θ-Al_2Cu. The presence of TiB_2 NPs in this θ-Al_2Cu phase leads to a less continuous network and thinner θ-Al_2Cu phase (Figure 5a, b). Also, the incorporation of NPs into the nanocomposite leads to the precipitation of the intermetallic Al_3Ti phase, highlighted by the arrows in Figure 5. EDS point analysis confirms the presence of Ti in points 2 and 3, while only Al and Cu are detected in the matrix (point 1 in Figure 5d). The Al_3Ti microprecipitate does not come from the Al-TiB_2 pellets, since a control casting using the lower Ti content B206 alloy as matrix and TiB_2 NPs as reinforcement showed no Al_3Ti phase in the microstructure (data not shown). Instead, we suspect that the fraction of TiB_2 NPs that are captured in the Al grain during solidification (shown in point 2 in Figure 5d) promote the nucleation of Al_3Ti microprecipitates (point 3 in Figure 5d) on their surface. This nucleation behavior of the Ti dissolved in the matrix on the TiB_2 surface has been previously observed for TiB_2 microparticles of 5−10 μm in diameter in pure Al systems.[33]

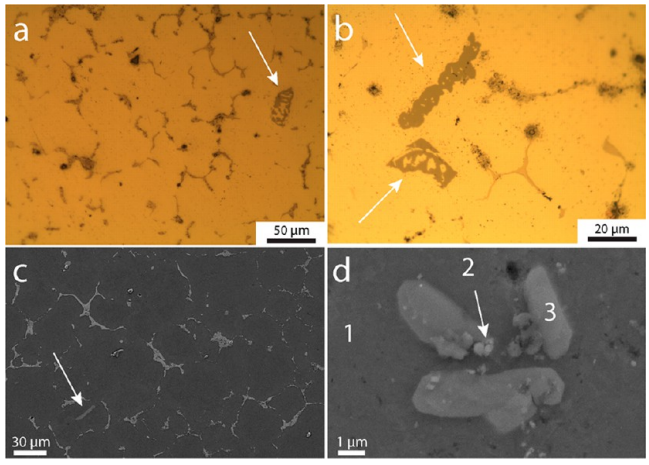

Figure 5. Optical (a, b) and SEM micrographs of the A206 + 1TiB_2 nanocomposite (sample ii).

The A206 + 0.2Mg + 0.1Ti + 1TiB_2 nanocomposite shows similar microstructure, also showing the intermetallic Al_3Ti phase precipitates and a fraction of the TiB_2 NPs pushed to the grain boundaries, together with the θ-Al_2Cu phase (Figure 6a).

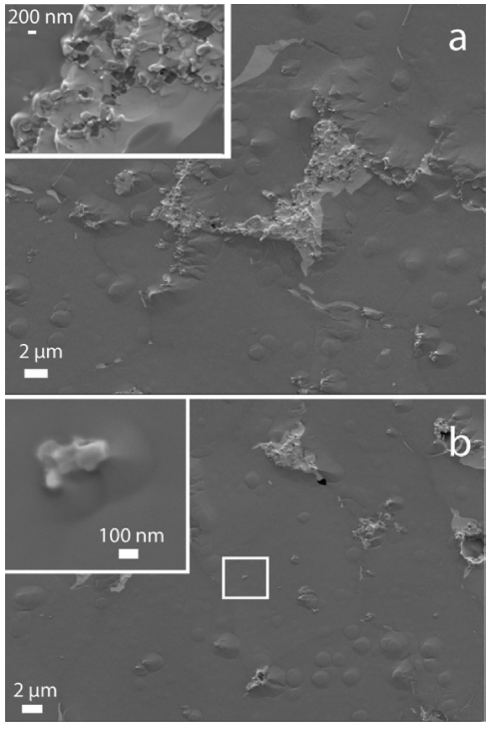

Figure 6. SEM micrographs of the A206 + 0.2Mg + 0.1Ti + 1TiB_2 nanocomposite (sample iv).

More interestingly, a significant fraction of TiB_2 NPs has been found to be captured within the primary Al grains (Figure 6b and inset). This behavior has not been previously observed in TiB_2-reinforced Al alloys prepared by solidification processing. EDS elemental mapping (Figure 7) confirms the Ti-rich nature of the captured NPs within the Al matrix.

The key parameters to achieve NP capture during metal solidification are the fundamental properties of the reinforcement NPs (e.g., Hamaker constant and electrical conductivity), as well as the absence of impurities on NP surface that might prevent capturing during solidification.[12] As shown in HRTEM in Figure 1c, the as-prepared TiB_2 NPs meet the latter requirement. With regard to the Hamaker constant (A), there is no known reinforcement material that would be spontaneously captured inside the grain, because of the relatively large A of Al (especially when compared to Mg melts). Thus, TiB_2 NP capture relies on the Brownian motion mechanism, which depends on the thermal energy of the NPs that are dispersed in the melt.[12] In short, capture by Brownian motion happens when the NP has enough thermal energy to overcome the van der Waals repulsion potential between the solid Al front and the NP. Our experimental findings show a fraction of TiB_2 NPs are captured, while some of them are still pushed to the grain boundary. These results are in good agreement with the Brownian motion mechanism, since only a fraction of NPs would be oscillating in the direction toward the Al solidification front. Higher NP loading could increase the fraction of NPs that are captured because of increased melt viscosity.[12]

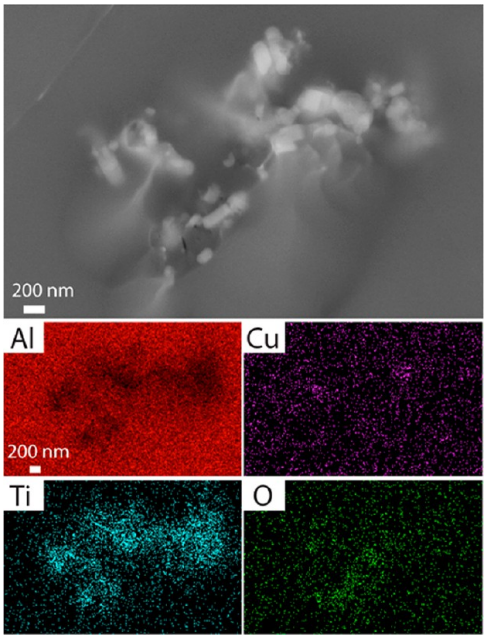

Figure 7. SEM and EDS elemental mapping of the A206 + 0.2Mg + 0.1Ti + 1TiB_2 nanocomposite (sample iv).

The average grain size has been measured from polarized light micrographs after electroetching the polished specimens in HBF_4 solution at a constant potential of 22 V for 20 s. The control A206 alloy has an average grain size of 331 ± 55 μm (Figure 8a). The average grain size is clearly reduced down to 45 ± 6 μm with the addition of 1 wt % TiB_2 NPs (Figure 8b). More importantly, the grain size distribution in the Control A206 sample is wide, showing a difference of more than 500 μm between the center and the edges of the sample. This undesirable behavior is caused by the difference in cooling rates between those areas. This effect is minimized in the as-prepared A206 + 1TiB_2 nanocomposite, which shows a much more homogeneous grain size distribution (Figure 8b). These results can be explained by the fact that the NPs act as nucleation agents for the primary Al grains, which results in increased number of grains and diminishes the coalescence into bigger grains, achieving a much smaller and homogeneous grain size. Furthermore, electron backscattering diffraction (EBSD) micrographs revealed that most of the primary Al grains have a misorientation larger than 15 degrees with respect to each other (blue boundaries, Supporting Information, Figure S1), demonstrating that the nanocomposite showed mostly high angle grain boundaries, a typical phenomenon for as-casted Al alloys. Moreover, it has also been found that there is some degree of refinement (average grain size, d = 137 ± 18 μm) provided by the intermetallic Al_3Ti phase that precipitates when additional 0.1 wt % Ti is added to the Control A206 (Figure 8c). Furthermore, smaller and more homogeneous grains are obtained for the A206 + 0.2Mg + 0.1Ti + 1TiB_2 nanocomposite, reaching an even smaller grain size of 30 ± 1 μm (Figure 8d), when combining the refining effect of TiB_2 NPs with additional Al_3Ti microprecipitates.

To evaluate the grain refinement capacity of the TiB_2 NPs, nanocomposite samples using B206 as the matrix were also prepared. As discussed above, the low Ti content of this alloy (<0.05 wt %) impedes the nucleation of Al_3Ti phase on the TiB_2 NPs surface, presenting a more clean-cut case to evaluate the refinement capacity of the TiB_2 NPs. The B206 alloy

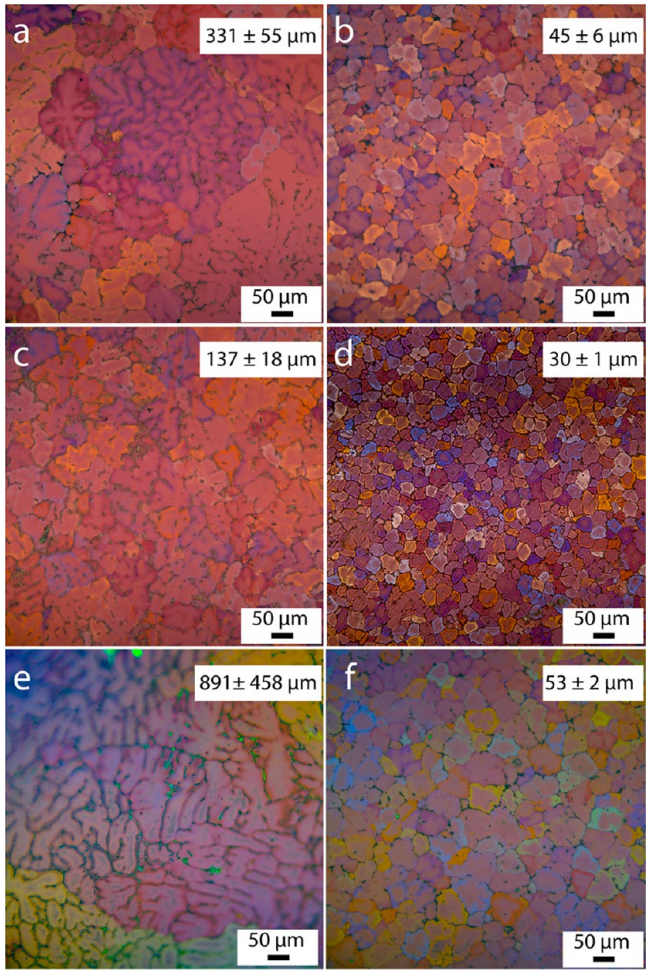

Figure 8. Polarized light optical micrographs of the as-prepared alloys and nanocomposites: A206 (a), A206 + 1TiB_2 (b), A206 + 0.2Mg + 0.1Ti (c), A206 + 0.2Mg + 0.1Ti + 1TiB_2 (d), Pure B206 alloy (e), and B206 + 1TiB_2 (f). The average grain size values are labeled.

showed large grains with a wide average size distribution (891 ± 458 μm, Figure 8e), while the addition TiB_2 NPs provided an effective refinement down to the average grain size of 53 ± 2 μm (Figure 8f). We attribute this behavior to the small size of TiB_2 NPs, which results in an increased number of nucleation sites, and thus smaller and more homogeneous Al grain size.

4. CONCLUSIONS

Surface-clean TiB_2 NPs with an average particle size of 20 nm have been synthesized by ultrasonic-assisted reduction of fluorotitanate and fluoroboride salts in molten Al at 700 °C. The as-prepared NPs are about 1 order of magnitude smaller than the particles prepared without ultrasonication. The role of the ultrasonic field is to restrict the particle size via acoustic cavitation effects. A master nanocomposite concept has been used to prepare A206-TiB_2 nanocomposites by solidification processing, avoiding the surface oxidation of the TiB_2 NPs to TiO_2, which results in superior incorporation and wetting behavior. Because of the high surface purity and small NP size, a significant fraction of the TiB_2 NPs have been captured within the primary Al grains, which was not previously achieved by solidification casting techniques in Al systems. Also, because of the small size of the TiB_2 NPs, the resulting TiB_2-reinforced Al nanocomposites show significant grain refinement.

■ ASSOCIATED CONTENT

Supporting Information

Electron backscattering diffraction (EBSD) micrograph of the TiB_2 nanocomposite. This material is available free of charge via the Internet at http://pubs.acs.org.

■ AUTHOR INFORMATION

Corresponding Author

*E-mail: jin@chem.wisc.edu. Fax: +1-608-262-0453. Phone: +1-608-262-1562.

Notes

The authors declare no competing financial interest.

■ ACKNOWLEDGMENTS

This research was supported by the U.S. Department of Commerce National Institute of Standards and Technology (NIST) through its Technology Innovation Program (Grant #70NANB10H003). The authors also acknowledge Daniel Hoefert and David Weiss from Eck Industries for their support on elemental analysis measurements.

■ REFERENCES

(1) Borgonovo, C.; Apelian, D. *Mater. Sci. Forum* **2011**, *678*, 1−22.
(2) Lloyd, D. J. *Int. Mater. Rev.* **1994**, *39*, 1−23.
(3) Koch, C. C.; Scattergood, R. O.; Murty, K. L. *JOM* **2007**, *59*, 66−70.
(4) Mortensen, A.; Jin, I. *Int. Mater. Rev.* **1992**, *37*, 101−128.
(5) Tjong, S. C.; Ma, Z. Y. *Mater. Sci. Eng., R* **2000**, *29*, 49−113.
(6) Rajan, T. P. D.; Pillai, R. M.; Pai, B. C. *J. Mater. Sci.* **1998**, *33*, 3491−3503.
(7) Delannay, F.; Froyen, L.; Deruyttere, A. *J. Mater. Sci.* **1987**, *22*, 1−16.
(8) Neuhaus, S.; Spencer, N. D.; Padeste, C. *ACS Appl. Mater. Interfaces* **2012**, *4*, 123−130.
(9) Isa, L.; Lucas, F.; Wepf, R.; Reimhult, E. *Nat. Commun.* **2011**, 2.
(10) Mortensen, A. *Mater. Sci. Eng., A* **1991**, *135*, 1−11.
(11) Lifshitz, E. M. *J. Exp. Theor. Phys.* **1956**, *2*, 73−83.
(12) Xu, J. Q.; Chen, L. Y.; Choi, H.; Li, X. C. *J. Phys.: Condens. Matter* **2012**, *24*, 255304.
(13) Carenco, S.; Portehault, D.; Boissière, C.; Mézailles, N.; Sanchez, C., *Chem. Rev.* **2013**, ASAP, DOI: dx.doi.org/10.1021/cr400020d.
(14) Han, Y. F.; Dai, Y. B.; Shu, D.; Wang, J.; Sun, B. D. *Appl. Phys. Lett.* **2006**, *89*, 144107.
(15) Weirauch, D. A.; Krafick, W. J.; Ackart, G.; Ownby, P. D. *J. Mater. Sci.* **2005**, *40*, 2301−2306.
(16) Mutale, C. T.; Krafick, W. J.; Weirauch, D. A. *Metall. Mater. Trans. B* **2010**, *41*, 1368−1374.
(17) Bates, S. E.; Buhro, W. E.; Frey, C. A.; Sastry, S. M. L.; Kelton, K. F. *J. Mater. Res.* **1995**, *10*, 2599−2612.
(18) Chen, L.; Gu, Y.; Qian, Y.; Shi, L.; Yang, Z.; Ma, J. *Mater. Res. Bull.* **2004**, *39*, 609−613.
(19) Hwang, Y.; Lee, J. K. *Mater. Lett.* **2002**, *54*, 1−7.
(20) Chen, Z. Y.; Chen, Y. Y.; Shu, Q.; An, G. Y.; Li, D.; Liu, Y. Y. *Metall. Mater. Trans. A* **2000**, *31*, 1959−1964.
(21) Li, P. T.; Li, Y. G.; Wu, Y. Y.; Ma, G. L.; Liu, X. F. *Mater. Sci. Eng., A* **2012**, *546*, 146−152.
(22) Emamy, M.; Mahta, M.; Rasizadeh, J. *Compos. Sci. Technol.* **2006**, *66*, 1063−1066.
(23) Langan, T. J.; Pickens, J. R. *Scripta Metall. Mater.* **1991**, *25*, 1587−1591.
(24) Dhokey, N. B. *Adv. Mater. Lett.* **2011**, *2*, 210−216.
(25) Choi, H.; Konishi, H.; Li, X. C. *Mater. Sci. Eng., A* **2012**, *541*, 159−165.
(26) Moldovan, P.; Butu, M.; Popescu, G.; Buzatu, M.; Usurelu, E.; Soare, V.; Mitrica, D. *Rev. Chim. (Bucharest, Rom.)* **2010**, *61*, 828−832.
(27) Lakshmi, S.; Lu, L.; Gupta, M. *J. Mater. Process. Technol.* **1998**, *73*, 160−166.
(28) Lu, L.; Lai, M. O.; Chen, F. L. *Adv. Compos. Mater.* **1997**, *6*, 299−308.
(29) Zhang, S. L.; Zhao, Y. T.; Cheng, X. N.; Chen, G.; Dai, Q. X. *J. Alloys Compd.* **2009**, *470*, 168−172.
(30) Wang, D. K.; De Cicco, M. P.; Li, X. C. *Mater. Sci. Eng., A* **2012**, *532*, 396−400.
(31) Watson, I. G.; Forster, M. F.; Lee, P. D.; Dashwood, R. J.; Hamilton, R. W.; Chirazi, A. *Composites, Part A* **2005**, *36*, 1177−1187.
(32) Choi, H.; Cho, W. H.; Konishi, H.; Kou, S.; Li, X. C. *Metall. Mater. Trans. A* **2013**, *44A*, 1897−1907.
(33) Mohanty, P. S.; Gruzleski, J. E. *Acta Metall. Mater.* **1995**, *43*, 2001−2012.